Direction Dynamics Study of the Hydrogen Abstraction Reaction $CH_2O + NH_2 \rightarrow CHO + NH_3$

Qian Shu Li* and Rui Hua Lü

School of Chemical Engineering and Materials Science, Beijing Institute of Technology, Beijing, 100081 China

Received: July 18, 2002; In Final Form: August 11, 2002

The hydrogen abstraction reaction $CH_2O + NH_2 \rightarrow CHO + NH_3$ has been studied using direct ab initio dynamics method. All of the information along the minimum energy path (MEP) was calculated at the UMP2/6-311+G(d, p) level of theory. Energetic data along the MEP were further refined using the scheme G2 with the UMP2/6-311+G(d, p) optimized geometries. The barrier heights for the forward and reverse reactions were obtained as 5.89 and 24.44 kcal/mol, respectively. Reaction rate constants and activation energies were calculated for the temperature range 250−2500 K by the improved canonical variation transition state theory (ICVT) incorporating a small-curvature tunneling correction (SCT). The rate constant at the room temperature was predicted to be 5.25×10^{-17} cm^3 molecule^{-1} s^{-1}, which is about 2 orders of magnitude smaller than that of the hydrogen abstraction reaction of acetaldehyde with aminogen.

Introduction

Formaldehyde is a key component in atmospheric chemistry and a key intermediate in hydrocarbon combustion. In the urban atmosphere, formaldehyde is mainly generated from automobile emissions. In the natural atmosphere, and especially in the stratosphere, it is thought to be a result of the oxidation of methane and other biogenic and anthropogenic hydrocarbons. Because of the importance of formaldehyde in the atmosphere, interstellar space, and combustion chemistry, a number of relevant kinetics investigations have been initiated since the 1970s.[1,2] The discovery of formaldehyde in the interstellar space and the recent measurements of its concentration in both the troposphere and stratosphere[3,4] provided further interest for its kinetic behavior. The reaction $CH_2O + NH_2 \rightarrow CHO + NH_3$ may play an important role in decreasing the depletion of ozone in the atmosphere and in minimizing the NO_x formation in the combustion process. Thus, a knowledge on the parameters around the kinetics is essential in modeling the corresponding chemical processes. To the best of our knowledge, although a series of hydrogen abstraction reactions of formaldehyde with radicals $CH_2O + X \rightarrow CHO + HX$ (X = F, Cl, Br, OH, and CN) has been extensively studied,[5−9] no experimental or theoretical data is as yet available for the $CH_2O + NH_2 \rightarrow CHO + NH_3$ reaction.

It is well-known that the direct ab initio dynamics method is a very useful means for predicting kinetics parameters of reactions,[10−12] which uses the electronic structure information, including the geometries, energies, gradients, and force constants (Hessians) at selected points along the reaction path, to calculate rate constants without the intermediate stage of constructing a full analytical potential energy surface (PES). The accuracy of the direct ab initio dynamics method depends on the precise description of the transition state and on the quality of the whole PES. Recent development of this method has opened up the possibility for detailed quantitative dynamical calculations of thermal rate constants of gas-phase chemical reactions. In the present study, the potential energy information and the rate constants have been calculated using the direct ab initio dynamics method employing the POLYRATE 8.2[13] program.

Computational Methods and Details

The computation of geometric parameters, harmonic vibrational frequencies, and the intrinsic reaction coordinate (IRC) was carried out using the Gaussian 98 package of programs.[14] As a reasonable compromise between speed and accuracy, all of the geometries of the reactants, products, and transition state have been fully optimized using the open shell second-order Møller−Plesset perturbation theory (UMP2)[15,16] with the 6-311+G(d, p) basis set. The MEP was calculated at the same level of theory based on the internal reaction coordinates with a step size of 0.02(amu)$^{1/2}$ bohr. A total of 75 points were located on each side of the IRC. At each selected point along the IRC, gradients and Hessians were calculated at the UMP2/6-311+G(d, p) level of theory. The single-point energy refinements were also carried out for the stationary points as well as for the selected points along the IRC at the CCSD(T)/6-311+G(3df, 2p)//UMP2/6-311+G(d, p) and G2//UMP2/6-311+G(d, p) levels of theory.

The rate constants at various temperatures were calculated using the conventional transition state theory (TST) and the improved canonical variational transition state theory (ICVT). Furthermore, the ICVT rate constants were corrected with the zero-curvature tunneling (ZCT) and the small-curvature tunneling (SCT) transmission coefficients.[11,17−23] All of the rate constant calculations were carried out using the general polyatomic rate constants code POLYRATE 8.2.[13]

Results and Discussion

A. Stationary Points. The optimized geometric parameters of the reactants (CH_2O and NH_2), products (CHO and NH_3), and the transition state at the UMP2/6-311+G(d, p) level of theory are listed in Table 1 together with the experimental values. The corresponding structures are displayed in Figure 1. For the reactants and products, this method yield excellent

* To whom correspondence should be addressed. Fax: +86-10-6891-2665. E-mail: qsli@mh.bit.edu.cn.

10.1021/jp026560x CCC: $22.00 © 2002 American Chemical Society
Published on Web 09/14/2002

TABLE 1: Optimized Geometries for the Reactants, Products, and Saddle Point for the $CH_2O + NH_2 \rightarrow CHO + NH_3$ Reaction at UMP2/6-311+G(d, p) Level, as Well as Experimental Values[a]

parameter	CH_2O	NH_2	CH_2ONH_2(TS)	CHO	NH_3
$r(O_1-C_2)$	1.213		1.189	1.183	
	$(1.203 \pm 0.003)^b$				
$r(C_2-H_3)$	1.105		1.115	1.122	
	$(1.099 \pm 0.009)^b$				
$r(N_5-H_6)$		1.025(1.024)[c,d]	1.025		1.013(1. 012)[d]
$r(C_2-H_4)$			1.242		
$r(N_5-H_4)$			1.379		
$\angle(O_1C_2H_3)$	121.9		124.0	124.3	
	$(121.75 \pm 0.6)^b$				
$\angle(O_1C_2H_4)$	121.9		123.3		
$\angle(H_3C_2H_4)$			112.7		
$\angle(H_6N_5H_7)$		102.8(103.0)[c,d]	104.1		107.4(106.7)[d]
$\angle(C_2H_4\,N_5)$			170.4		
$\tau(H_3C_2N_5H_7)$			178.6		

[a] Bond lengths are expressed in angstroms, and angles are in degrees. The values in parentheses are experimental values. [b] Reference 24. [c] Reference 25. [d] Reference 26.

TABLE 2: Heat of Reaction and Barrier Heights (kcal/mol) for the $CH_2O + NH_2 \rightarrow CHO + NH_3$ Reaction[a]

levels	$\Delta_r H^0_{298K}$	$V_f^{\ddagger}$	$V_{fa}^{G\ddagger}$	$V_r^{\ddagger}$	$V_{ra}^{G\ddagger}$
UMP2/6-311+G(d,p)	−21.18	10.26	10.52	32.50	31.71
QCISD/6-311+G(d,p)	−16.82				
CCSD(T)//6−311+G(3df,2p)//UMP2/6-311+G(d,p)	−18.15	6.76	7.03	25.98	25.19
G2// UMP2/6-311+G(d,p)	−18.54	6.31	5.89	25.78	24.44
expt[b]	-19.79 ± 0.39				

[a] $V_{fa}^{G\ddagger}$ forward reaction potential barriers with zero-point energy (ZPE) correction. $V_{ra}^{G\ddagger}$ reverse reaction potential barriers with zero-point energy (ZPE) correction. [b] Based on available experimental data in ref. 28.

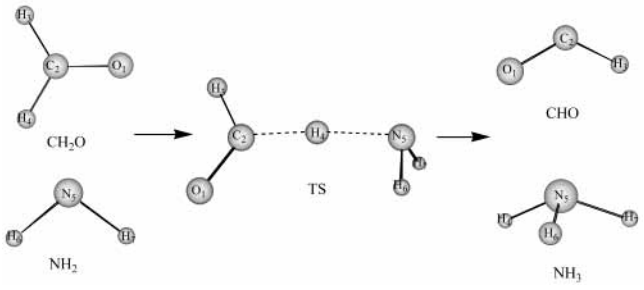

Figure 1. Optimized geometries of the stable points and transition state.

agreement with the experimental data.[24−26] In particular, the maximum deviations are only 0.01 Å for bond lengths and 0.7° for bond angles, indicating that the UMP2/6-311+G(d, p) method is suitable to depict the structures involved in the reaction. From Figure 1, it can be seen that the transition state has a C_1 symmetry. The bond length C_2-H_4, which is breaking, increases by 12.4%, and the bond length H_4-N_5, which is forming, increases by 36.1% with respect to the equilibrium bond lengths in CH_2O and NH_3. The resemblance of the structures between the reactants and the transition state indicate that the transition state appears earlier on the reaction path, as can be anticipated for exothermic reactions.[27] In addition, the geometry predicted for the transition state is nearly collinear with regard to the angle between the breaking C_2-H_4 bond and the forming H_4-N_5 ($<C_2H_4N_5 = 170.4$) bond.

The reaction enthalpies and barrier heights of the title reaction are listed in Table 2. It is obvious that the zero-point energy (ZPE) corrected reaction energy from the G2 method (−18.54 kcal mol^{-1}) provides the best result among all of the methods employed in this study when compared with the experimental reaction enthalpy[28] (-19.79 ± 0.39 kcal mol^{-1}). The calculated ZPE corrected reaction energies at the UMP2/6-311+G(d, p), CCSD(T)/6-311+G(3df,2p)//UMP2/6-311+G(d, p), and QCISD/6-311+G(d, p) levels of theory are −21.18, −18.15, and −16.82 kcal/mol, respectively. It can also be seen from Table 2 that the calculated barrier heights are sensitive to the computational methods. The calculated ZPE corrected barriers for the forward reaction ($V_{fa}^{G\ddagger}$) are 10.52, 7.03, and 5.89 kcal/mol, using the UMP2/6-311+G(d, p), CCSD(T)/6-311+G(3df, 2p)//UMP2/6-311+G(d, p), and G2//UMP2/6-311+G(d, p) methods, respectively. The ZPE corrected barrier heights for the reverse reaction are 31.71, 25.19, and 24.44 kcal/mol, using the same methods, respectively. It is noticed that the CCSD(T)/6-311+G-(3df, 2p)//UMP2/6-311+G(d, p), and G2//UMP2/6-311+G(d, p) methods provide close reaction energies and barrier heights. Considering the fine agreement between the reaction energy calculated using the G2//UMP2/6-311+G(d, p) method and the experimental reaction enthalpy,[28] it can be concluded that either the CCSD(T)/6-311+G(3df, 2p)//UMP2/6-311+G(d, p) or the G2//UMP2/6-311+G(d, p) method is required to give more accurate energetic data in the present study.

The harmonic vibrational frequencies and the zero-point energies (ZPE) for the reactants (CH_2O, NH_2), products (CHO, NH_3), and transition state **(**HO $C_2\cdots H_4\cdots N_5H_7H_8$**)** calculated at the UMP2/6-311+G(d, p) level of theory are listed in Table 3 together with the available experimental frequencies[25,26,29−31] of reactants and products. The maximum error for the theoretical vibrational frequencies is within 12.8% compared with the corresponding experimental values.[25,26,29−31] Notice that the absolute value of the imaginary frequency is quite large (2319*i*), which implicates that a significant tunneling effect may occur at low temperatures.

B. Reaction Path Properties. Figure 2 shows the variations of bond distances with the reaction coordinate of the reaction $CH_2O + NH_2 \rightarrow CHO + NH_3$. It can be seen that the bond lengths of C_2-H_4 and H_4-N_5 change dramatically with the intrinsic reaction coordinate *s*. On the other hand, bond lengths of all of the other bonds change little. As the reaction proceeds from reactants to products (i.e., *s* changes from $-\infty$ to $+\infty$), the breaking bond distance (C_2-H_4) remains practically un-

TABLE 3: Harmonic Vibrational Frequencies (cm^{-1}) and Zero-Point Energies (ZPE; Kcal mol^{-1}) at the UMP2/6-311+G(d, p) Level, as Well as Experimental Values

frequencies	UMP2/6-311+G(d, p)									experiment						ZPE
CH_2O	3047	2976	1762	1588	1278	1206				3009	2944	1764	1563	1191	1287[a]	16.88
NH_2	3559	3459	1519							3220	3173	1497 [b,c]				12.18
CHO	2755	1947	1120							2442	1856	1076[d]				8.31
NH_3	3682	3682	3529	1661	1661	1060				3577	3577	3506	1691	1691	1022[c,e]	21.80
TS	3558	3448	2914	2264	1561	1518	1341									29.32
	1341	1251	841	720	637	282	149	59	2319i							

[a] Reference 29. [b] Reference 25. [c] Reference 26. [d] Reference 30. [e] Reference 31.

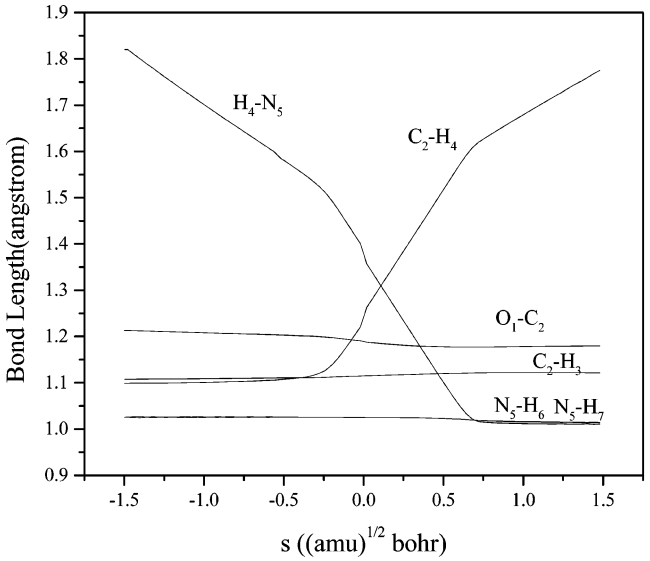

Figure 2. Changes of the bond distances (in Å) as a function of the intrinsic reaction coordinate s $(amu)^{1/2}$ bohr at the UMP2/6-311+G-(d,p) level.

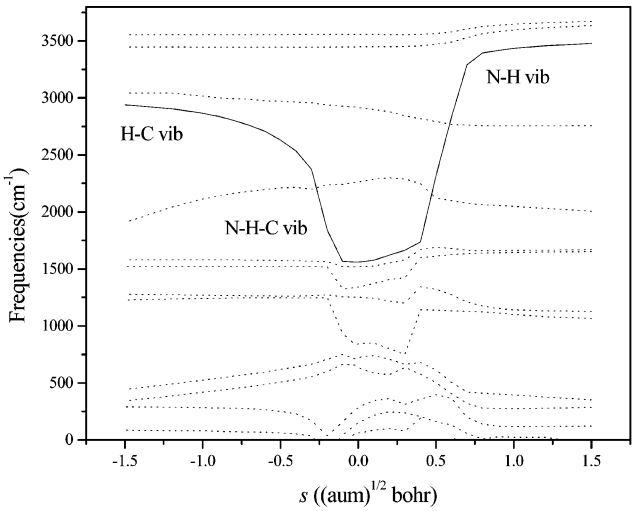

Figure 3. Generalized normal mode vibrational frequencies as a function of the intrinsic reaction coordinate s $(amu)^{1/2}$ bohr at the UMP2/6-311+G(d,p) level.

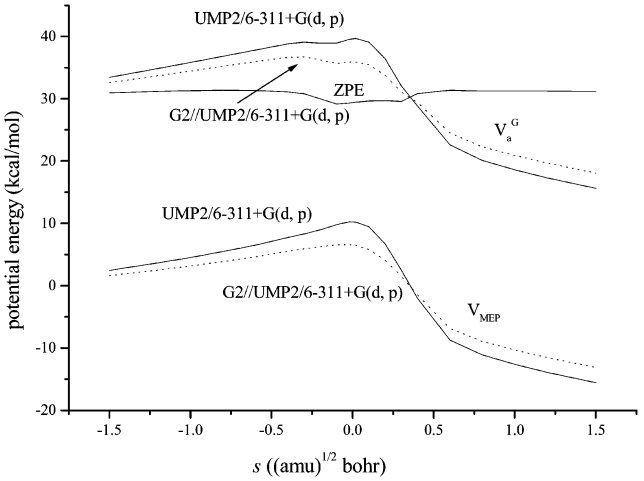

Figure 4. Curves of potential energy (V_{MEP}) and vibrationally adiabatic ground-state potential energy (V_a^G) as a function of the intrinsic reaction coordinate s $(amu)^{1/2}$ bohr.

changed until the reaction coordinate s reaches -0.25 $(amu)^{1/2}$ bohr, where it starts to increase almost linearly with s. Synchronously with this, the forming bond length (H_4-N_5) decreases almost linearly until s reaches about $+0.75$ $(amu)^{1/2}$ bohr. At this point, the H_4-N_5 bond is formed, and the bond length remains changed afterward. Thus, the region from $s = -0.25$ to 0.75 $(amu)^{1/2}$ bohr on the IRC dominates the shuttling of the hydrogen atom from the carbon atom to the nitrogen atom.

The curves of the generalized frequencies calculated at the UMP2/6-311G+(d, p) level of theory are plotted in Figure 3 with respect to the reaction coordinate. At both the reactants asymptote ($s = -\infty$) and the products asymptote ($s = +\infty$), vibrational frequencies of the reacting system change to the corresponding vibrational frequencies of reactants and products, respectively. The solid line shown in Figure 3 denotes the harmonic $C_2\cdots H_4\cdots N_5$ stretching vibration. When $s < 0$ $(amu)^{1/2}$ bohr, this mode is the stretching vibration mode of the breaking C_2-H_4 bond of CH_2O, and when $s > 0$ ($amu^{1/2}$) bohr, this mode is the stretching vibrational mode of the forming H_4-N_5 bond of NH_3. This character indicates that the vibrational mode ν-($C_2\cdots H_4\cdots N_5$) is closely related to the hydrogen abstraction reaction, so the vibrational mode $\nu(C_2\cdots H_4\cdots N_5)$ can be referred to as the "reaction mode".

The classical potential energy $V_{MEP}(s)$ and the ground-state adiabatic potential energy $V_a^G(s)$ at UMP2/6-311+G(d, p) and G2//UMP2/6-311+G(d, p) levels of theory are plotted in Figure 4 for the reaction $CH_2O + NH_2 \rightarrow CHO + NH_3$. From Figure 4, it can be seen that both the V_{MEP} at UMP2/6-311+G(d, p) and G2//UMP2/6-311+G(d, p) levels of theory are well established, and the maxima of both V_{MEP} have no obvious shifting. The curve of V_a^G is quite different from the curve of V_{MEP}. Because V_a^G is a consequence of summing up V_{MEP} and ZPE, due to a significant drop of ZPE prior to the saddle point zone, the curve of V_a^G of UMP2/6-311+G(d, p) and G2//UMP2/6-311+G(d, p) methods also exhibits two barriers. For the $V_a^G(s)$ of the UMP2/6-311+G(d, p) method, one barrier, higher in energy, is located at the original transition state at $s = 0$, and the other barrier is located in the entrance valley at $s = -0.30$ $(amu)^{1/2}$ bohr. However, for the $V_a^G(s)$ of the G2//UMP2/6-311+G(d, p) method, the higher barrier is shifted to the entrance valley at approximately $s = -0.30$ $(amu)^{1/2}$ bohr and the other at the original transition state at $s = 0$. Espinosa-Garcia and Corchado[32] have argued that this kind of shifting is

TABLE 4: Bottleneck Properties (ICVT) of the Reaction

T	s	V_{MEP}	V_a^G	T	s	V_{MEP}	V_a^G
S. P.	0.000	6.54	35.91	398	0.057	6.23	35.75
250	0.031	6.41	35.86	400	0.057	6.23	35.75
268	0.034	6.39	35.85	500	0.070	6.11	35.67
273	0.035	6.38	35.85	550	0.076	6.06	35.64
278	0.036	6.38	35.85	600	0.080	6.02	35.61
295	0.039	6.36	35.83	650	0.083	5.99	35.58
298	0.039	6.35	35.83	700	0.087	5.95	35.55
318	0.043	6.33	35.82	723	0.088	5.94	35.54
335	0.046	6.31	35.80	800	0.092	5.89	35.50
336	0.046	6.30	35.80	1000	0.101	5.79	35.42
346	0.048	6.29	35.80	1250	0.109	5.68	35.33
353	0.049	6.28	35.79	1500	0.116	5.60	35.25
363	0.051	6.27	35.79	1750	0.121	5.52	35.18
370	0.052	6.26	35.78	2000	0.126	5.46	35.12
377	0.053	6.26	35.77	2500	0.132	5.36	35.02

TABLE 5: Activation Energies (in kcal/mol) for the Title Reaction

lower T	upper T	TST	CVT	ICVT	CVT/SCT	ICVT/SCT
250	268	6.86	6.76	6.81	4.97	4.65
268	298	6.95	6.82	6.86	5.30	5.00
298	335	7.07	6.9	6.93	5.62	5.34
335	398	7.29	7.08	7.10	6.03	5.75
400	500	7.70	7.40	7.42	6.60	6.31
500	800	8.76	8.29	8.30	7.90	7.48
800	1500	11.65	10.93	10.94	11.02	10.45
1500	2500	17.05	16.03	16.03	16.55	15.75

caused artificially by the computational technique, namely, optimizing geometries at a lower level of theory (MP2) and then refining the energies (without re-optimization) at a higher level of theory (G2). For a further understanding of the variational effect, dynamics bottleneck properties of the reaction based on the improved canonical variational transition state approach (ICVT) are listed in Table 4. It can be seen that the position of the variational transition state shifts to the product direction on the IRC when temperature increases. The variational transition state shifts to 0.1324 $(amu)^{1/2}$ bohr at 2500 K. These results show that there exist considerable variational effects in the title reaction.

C. Rate Constants. On the basis of the G2//UMP2/6-311+G-(d, p) energies, we calculated the rate constants using the TST, ICVT, and ICVT/SCT methods. The results are shown in Figure 5a. It is seen that deviations of rate constants between TST and ICVT increase with increments in temperature. This indicates that the variational effects increase as temperature rises and is in agreement with the discussion in the previous section. Thus, the variational approach is required to calculate the rate constants at higher temperature (>500 K) for the title reaction. By comparing the rate constants of ICVT, ICVT/ZCT, and ICVT/SCT, it can be seen that the tunneling effects is important in a large temperature range (<600 K). In particular, the SCT correction for tunneling effects is required at low temperatures.

Figure 5b depicts the ICVT/SCT rate constants calculated from UMP2/6-311+G(d, p), CCSD(T)/6-311+G(3df, 2p)//UMP2/6-311+G(d, p), and G2//UMP2/6-311+G(d, p) energies. Obviously, the rate constants predicted from UMP2/6-311+G-(d, p) energies are not qualified as a result of over-estimations in the barrier height. The rate constants calculated from CCSD-(T)/6-311+G(3df, 2p)//UMP2/6-311+G(d, p) and G2//UMP2/6-311+G(d, p) energies are in good agreement with each other.

Table 5 lists the activation barriers that are estimated from the ICVT/SCT rate constants in several temperature range. In the temperature range 298−335 K, the activation energy is 5.34 kcal/mol. Although there is no experimental activation energy

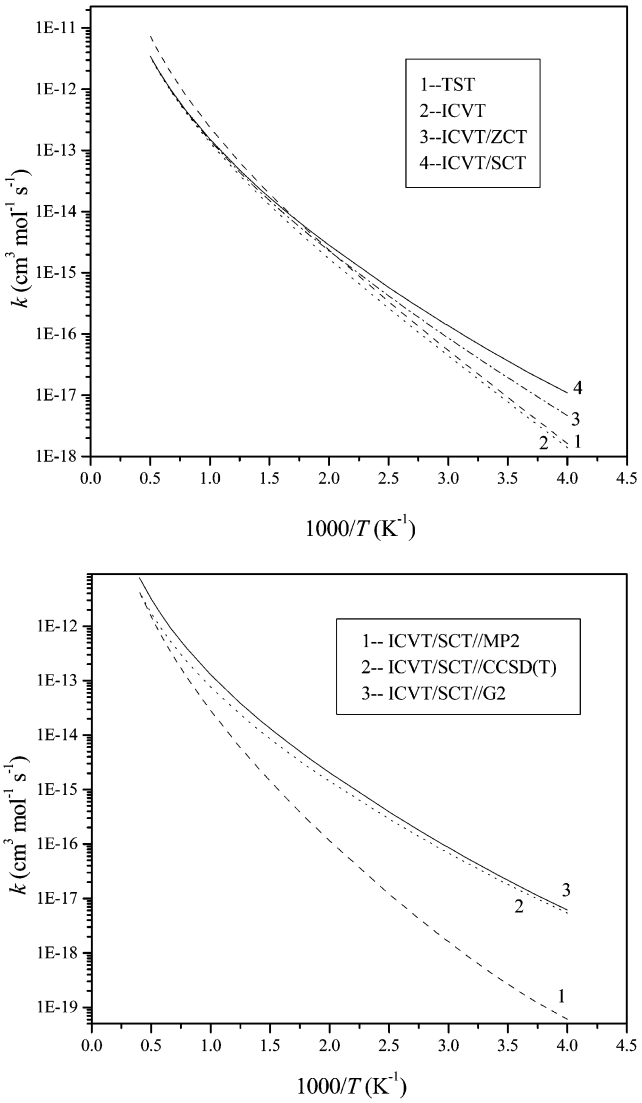

Figure 5. a. Forward reaction rate constants k (in cm^3 $molecule^{-1}$ s^{-1}) as a function of the reciprocal of the temperature (in K^{-1}) in the range 250−2500 K. The dash line (1) denotes the rate constants calculated from conventional transition state theory (TST). The dot line (2) denotes the rate constants calculated from improved canonical variational transition state theory (ICVT). The dash dot line (3) denotes the rate constants calculated from ICVT incorporating zero-curvature tunneling (ZCT) correction. The solid line (4) denotes the rate constants calculated from ICVT incorporating small-curvature tunneling (SCT) correction. b. Forward reaction rate constants k (in cm^3 $molecule^{-1}$ s^{-1}) at three different levels of theory in the range 250−2500 K.

to compared with, the values seem to be reasonably based on the activation energy of the reaction $CH_3CH_2O + NH_2 \rightarrow CH_3$-$CHO + NH_3$ in the temperature range 297−548 K[33] and the methyl effect on hydrogen abstraction of alkane with amino-gen.[34,35]

Summary

In this study, we have presented a detailed analysis on the reaction paths and rate constants for the reaction $CH_2O + NH_2 \rightarrow CHO + NH_3$. We used the UMP2/6-311+G(d, p)[15,16] method to calculate the geometries and frequencies along the reaction paths and then obtained the information of PES with the same method. The refined barrier height at the G2 //UMP2/6-311+G-(d, p) level of theory is 5.89 kcal mol^{-1}.

By analyzing the minimum energy reaction paths, it is found that the hydrogen abstraction process mainly occurs in the range

of $-0.25 \sim +0.75$ (amu)$^{1/2}$ bohr on the MEP of the reaction. During the reaction processes, the C_2-H_4 bond is breaking, the H_4-N_5 bond is forming, while the C_2-H_4 stretching vibrational mode gradually changes to the H_4-N_5 stretching vibrational mode.

The rate constants and the activation energies are calculated in the temperature range of 250−2500 K using the improved canonical variational transition state theory, incorporating zero-curvature tunneling and small-curvature tunneling corrections. The results of the calculations indicate that variational effects on the rate constants are obvious at higher temperatures, whereas the tunneling corrections are very important for the rate constants at low temperatures, and the effect of the SCT is more significant than that of the ZCT. The rate constants for the title reaction are 5 orders of magnitude smaller than those reactions of formaldehyde with F, Cl, Br, CN, and OH[5−9,36] in the low-temperature range, whereas in the high-temperature range, their rate constants are much closer.

Acknowledgment. We thank Professor D. G. Truhlar for providing the POLYRATE 8.2 program. We thank Dr. S. W. Zhang for his useful help. This work is supported by the National Science Foundation of China.

Supporting Information Available: Table showing the forward rate constants for the title reaction. This material is available free of charge via the Internet at http://pubs.acs.org.

References and Notes

(1) Houston, P. L.; Moore, C. B. *J. Chem. Phys.* **1976**, *65*, 757.

(2) Moore, C. B.; Weisshaar, J. C. *Annu. Rev. Phys. Chem.* **1983**, *34*, 525.

(3) Barbe, A.; Marche, P.; Secroun, C.; Jouve, P. *Geophys. Res. Lett.* **1979**, *6*, 463.

(4) Zhou, X.; Lee, Y.-N.; Newman, L.; Chen, X. *J. Geophys. Res.* **1996**, *101*, 14.

(5) Beukes, J. A.; Anna, B. D.; Bakken, V.; Nielsen, C. J. *Phys. Chem. Chem. Phys.* **2000**, *2*, 4049.

(6) Michael, J. V.; Nava, D. F.; Payne, W. A.; Stief, L. J. *J. Chem. Phys.* **1979**, *70*, 1147.

(7) Feng, W. L.; Wang, Y.; Zhang, S. W.; Pang, X. Y. *Chem. Phys. Lett.* **1997**, *266*, 43.

(8) Butkovskaya, N. I.; Setser, D. W. *J. Phys. Chem. A* **1998**, *102*, 9715.

(9) Poulet, G., Laverdet, G., Bras, G. L. *J. Phys. Chem.* **1981**, *85*, 1892.

(10) Truhlar, D. G. Direct Dynamics Method for the Calculation of Reaction Rates. In *The Reaction Path in Chemistry: Current Approaches and Perspectives*; Heidrich, D., Ed.; Kluwer: Dordrecht, 1995; pp 229−225.

(11) Truhlar, D. G.; Garrett, B. C.; Klippenstein, S. J. *J. Phys. Chem.* **1996**, *100*, 12771.

(12) Hu, W.-P.; Truhlar, D. G. *J. Am. Chem. Soc.* **1996**, *118*, 860.

(13) Chuang, Y. Y.; Corchado, J. C.; Fast, P. L.; Villà, J.; Hu, W.-P.; Liu, Y.-P.; Lynch, G. C.; Jackels, C. F.; Nguyen, K. A.; Gu, M. Z.; Rossi, I.; Isaacson, E. L.; Truhlar, D. G. *Polyrate*, version 8.2; University of Minnesota: Minneapolis, MN, 1999.

(14) Frisch, M. J.; Trucks, G. W.; Schlegel, H. B.; Scuseria, G. E.; Robb, M. A.; Cheeseman, J. R.; Zakrzewski, V. G.; Montgomery, J. A., Jr.; Stratmann, R. E.; Burant, J. C.; Dapprich, S.; Millam, J. M.; Daniels, A. D.; Kudin, K. N.; Strain, M. C.; Farkas, O.; Tomasi, J.; Barone, V.; Cossi, M.; Cammi, R.; Mennucci, B.; Pomelli, C.; Adamo, C.; Clifford, S.; Ochterski, J.; Petersson, G. A.; Ayala, P. Y.; Cui, Q.; Morokuma, K.; Malick, D. K.; Rabuck, A. D.; Raghavachari, K.; Foresman, J. B.; Cioslowski, J.; Ortiz, J. V.; Stefanov, B. B.; Liu, G.; Liashenko, A.; Piskorz, P.; Komaromi, I.; Gomperts, R.; Martin, R. L.; Fox, D. J.; Keith, T.; Al-Laham, M. A.; Peng, C. Y.; Nanayakkara, A.; Gonzalez, C.; Challacombe, M.; Gill, P. M. W.; Johnson, B. G.; Chen, W.; Wong, M. W.; Andres, J. L.; Head-Gordon, M.; Replogle, E. S.; Pople, J. A. *Gaussian 98*; Gaussian, Inc.: Pittsburgh, PA, 1998.

(15) Møller, C.; Plesset, M. S. *Phys. Rev.* **1934**, *46*, 618.

(16) Head-Gordon, M.; Pople, J. A.; Frisch, M. J. *Chem. Phys. Lett.* **1988**, *153*, 503.

(17) Truhlar, D. G.; Isaacson, A. D.; Garrett, B. C. In *The Theory of Chemical Reaction Dynamics*; Baer, M., Ed.; CRC Press: Boca Raton, FL, 1985; Vol. 4, p 65.

(18) Truhlar, D. G.; Kuppermann, A. *J. Chem. Phys*. **1970**, *52*, 3841.

(19) Garrett, B. C.; Truhlar, D. G.; Grev, R. S.; Magnuson, A. W. *J. Phys. Chem*. **1980**, *84*, 1730.

(20) Steckler, R.; Hu, W.-P.; Liu, Y.-P.; Lynch, G. C.; Garrett, B. C.; Isaacson, A. D.; Melssas, V. S.; Lu, D.-H.; Truong, T. N.; Rai, S. N.; Hancock, G. C.; Lauderdale, J. C.; Joseph, T.; Truhlar, D. G. *Comput. Phys. Commun*. **1995**, *88*, 491.

(21) Duncan, W. T.; Bell, R. L.; Truong, Y. N. *J. Comput. Phys*. **1998**, *19*, 1039.

(22) Truong, T. N.; Truhlar, D. G. *J. Chem. Phys*. **1990**, *93*, 1761.

(23) Liu, Y.-P.; Lynch, G. C.; Truong, T. N.; Lu, D.-H.; Truhlar, D. G.; Garret, B. C. *J. Am. Chem. Soc*. **1993**, *115*, 2408.

(24) Yamada, K.; Nakagawa, T.; Kuchitsu, K.; Morino, Y. *J. Mol. Spectrosc.* **1971**, *38*, 70.

(25) Harmony, M. D.; Schwendeman, M. D.; Laurie, V. W.; Kuczkowski, R. L.; Schwendeman, R. H.; Ramsay, D. A.; Lovas, F. J.; Larfferty, W. J.; Maki, A. G. *J. Phys. Chem. Ref. Data.* **1979**, *8*, 619.

(26) Chase, M. W., Davies, C. A., Jr., Downey, J. R., Fruip, D. J., McDonald, R. A., Eds.; JANAF Thermochemical Tables, 3rd ed.; Natl. Stand. Ref. Data Ser., vol.14; Natl. Bur. Stand.: Washington, DC, 1985.

(27) Hammond, G. S. *J. Am. Chem. Soc.* **1963**, *85*, 3239

(28) Atkinson, R.; Baulch, D. L.; Cox, R. A.; Hampson, R. F., Jr.; Kerr, J. A.; Rossi, M. J.; Troe, J. *J. Phys. Chem. Ref. Data.* **1999**, *28*, 391.

(29) Duncan, J. L.; Mallinson, P. D. *Chem. Phys. Lett.* **1973**, *23*, 597.

(30) Pettersson, M.; Khriachtchev, L.; Jolkkonen, S.; Rasanen, M. *J. Phys. Chem. A* **1999**, *103*, 9154

(31) Miller, K. J.; Ganda-Kesuma, F. S. *J. Mol. Spectrosc*. **1991**, *145*, 429.

(32) Espinosa-Garcia, J.; Corchado, J. C. *J. Phys. Chem.* **1995**, *99*, 8613.

(33) Hack, W.; Kurzke, H.; Rouveirolles, P.; Wagner, H. G. *Ber. Bunsen-Ges. Phys. Chem.* **1986**, *90*, 1210.

(34) Yu, Y. X.; Li, S. M.; Xu, Z. F.; Li, Z. S.; Sun, C. C. *Chem. Phys. Lett.* **1998**, *296*, 131.

(35) Yu, Y. X.; Li, S. M.; Xu, Z. F.; Li, Z. S.; Sun, C. C. *Chem. Phys. Lett.* **1999**, *302*, 281.

(36) Baulch, D. L.; Cobos, C. J.; Cox, R. A.; Esser, C.; Frank, P.; Just, Th.; Kerr, J. A.; Pilling, M. J.; Troe, J.; Walker, R. W.; Warnatz, J. *J. Phys. Chem. Ref. Data.* **1992**, *21*, 411.